RESEARCH ARTICLE

Probabilistic assessment of storm surge potential due to explosive cyclogenesis in the northwest Pacific region

A. Saruwatari[a], K. Fukuhara[a] and Y. Watanabe[a]

[a]Faculty of Engineering, Hokkaido University, N13 W8, Sapporo, Japan

ABSTRACT

Extratropical cyclones that develop rapidly in the northwest Pacific Ocean, called explosive cyclones, have caused storm surges twice recently along the coast of Nemuro Bay, located in northeastern Japan, in 2014 and 2015. As the number and intensity of explosive cyclones have increased over the last three decades near the Japanese archipelago (Iwao, Inatsu, and Kimoto 2012), the frequency of extreme storm surges is anticipated to increase under future climatic conditions. Explosive cyclones formed in the northwest Pacific region can be categorized into three major types (Yoshida and Asuma 2004) based on their evolution: Type-I cyclones develop over the Sea of Japan and travel toward the Sea of Okhotsk, Type-II are generated on the continent and move toward the Pacific Ocean through the Sea of Japan, and Type-III travel northward in the Pacific Ocean along the Japanese archipelago. We performed computational experiments of past storm surges to find statistical fea-tures of local sea levels, depending on the types of the cyclone evolution under a realistic meteorological scenario of winter cyclones, with aim to provide possible sea level rise expected in the northeast Asia.

Here, we show that amplification of local sea level, governed by the orientation of coastal lines with cyclone tracks, is defined by the evolution type that is classified by their trajectories, rather than the intensity, of the cyclone. Nemuro Bay is the most vulnerable site in the northwest Pacific region regardless of the evolution type; thus repeated disasters are anticipated therein. Severe storm surges are also expected along certain other semi-enclosed coasts facing the northern Sea of Japan and Sea of Okhotsk due to Type-I cyclones. The probabilistic evaluation of sea levels depending on the cyclone evolution type as introduced in this study may be useful for evaluating potential disasters.

KEYWORDS

Storm surge; explosive cyclogenesis; winter storms; MIT general circulation model

CONTACT A. Saruwatari. Email: saruwata@eng.hokudai.ac.jp

1. Introduction

Extratropical cyclones that rapidly intensify during the winter monsoon in the northwestern Pacific Ocean or northwestern Atlantic Ocean often develop into explosive cyclones. The past explosive cyclones have severely impacted human activities due to extreme wind, waves and precipitation, as often reported on the east coasts of the Eurasian and North American continents (e.g. Sanders 1986; Gyakum and Danielson 2000; Kocin et al. 1995). In 2014, an energetic explosive cyclone intensified in the northwestern Pacific Ocean, traveled north, and induced a storm surge with a 2-m sea level rise in Nemuro Bay on the east coast of Hokkaido (see **Figure 1**); it caused $20 million of damage due to flooding in the central area of Nemuro city (Saruwatari et al. 2015). A comparable cyclone passed through the same area in 2015, causing the sea level in the bay to rise again. These successive storm surges at the same location suggest that storm surge risk is associated with the similarity in the cyclone trajectory that is dominated by the large-scale distribution of the air masses in this region, as well as with the topographical vulnerability of the coast.

Over the past three decades, the frequency of intensified explosive cyclones near the Japanese archipelago has increased (Iwao, Inatsu, and Kimoto 2012), and future disasters are anticipated to occur with greater frequency if the same trend continues. However, the mechanism of storm surges driven by the explosive cyclones have been poorly understood because of less research attention in this field since past explosive cyclones never caused significant surge disaster in this area before the 2014 Nemuro event. After the disaster, Kumagai et al. (2017) performed a hindcasting computation of transitional surge and wave systems during the travel of the 2014 explosive cyclone. Bricker et al. (2015) estimated possible damage extensions for a hypothetical storm with 150% the intensity of the 2014 cyclone as a possible effect of climate change. However realistic scenarios statistically supported by regional meteorological features of the explosive cyclones are required to assess probabilistic sea level rise and possible disaster.

The evolution of explosive cyclones, observed in the northeast Asia, highly depends on the baroclinic effects of the monsoon; growth of the Siberian High, inducing baroclinicity in the Sea of Japan, is an important factor to determine the tracks and intensities of the winter cyclones. In addition, warm ocean currents also affect frequencies of the explosive cyclongenesis (Sanders and Gyakum 1980), and in particular, heat energy from Kuroshio Current contributes to grow the cyclones generated in the northwest Pacific Ocean (Kuwano-Yoshida and Asuma 2008; Chen et al. 1992). These effects cause annual variations in local developments of the cyclones. Yoshida and Asuma (2004) identified three major evolution types of the past explosive cyclones in the northwest Pacific Ocean, including cyclones that: (Type I) achieve their maximum growth in the Sea of Japan or Sea of Okhotsk, (Type II) form on the Eurasian continent or the Sea of Japan and achieve their maximum growth in the Pacific Ocean, (Type III) or form over the Pacific Ocean and achieve their maximum growth in the Pacific Ocean.

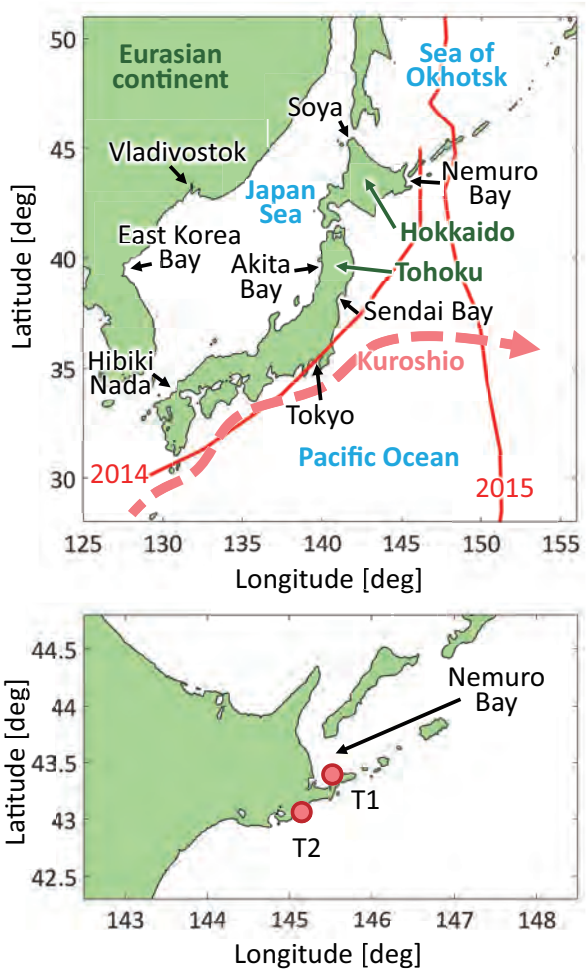

Figure 1. Map of the northwest Pacific region together with the names of the representative semi-enclosed coastal sites (top) and magnified map around Nemuro Bay (bottom). Two red lines in the top figure show the trajectories of the cyclones that caused the Nemuro storm surges in 2014 and 2015.

It is generally known that characteristics of storm surges are sensitive to a local wind system near coasts. Accordingly meteorologically defined patterns of cyclone tracks and growth processes may also characterize local surge responses, which has been verified in the northern Brazil (Parise, Calliari, and Krusche 2009) and the northeast coasts of the US (Catalano and Broccoli 2018). The classification by Yoshida and Asuma (2004) is thus useful for identifying the evolution type of cyclones that cause local storm surges along coasts of the northwest Pacific Ocean.

This study aims to provide a probabilistic assessment of storm surges on the basis of statistical features of past explosive cyclones classified in the above meteorological categories through computational experiments. In this paper, three-dimensional ocean current computations were performed to obtain local sea level rise along the coasts of Japan and Eurasia for cyclones observed in the past two decades. The vulnerability of local coasts and disaster risks are discussed in relation to the calculated probability of sea level rise due to potential storm surges.

This paper is organized as follows. Section 2 describes the statistical features of explosive cyclones based on evolution type. The computational models used in this study are explained, along with model validation through hindcasting of the 2014 Nemuro storm surge in Section 3. In Section 4, probabilistic sea level rises, forced by ensemble cyclones as well as previous storms sampled over the last two decades, are discussed in terms of coastal vulnerability and the disaster risks associated with storm surges. Finally, our findings are summarized in Section 5.

2. Explosive Cyclones in the Northwest Pacific Ocean

In this study, the explosive cyclone is defined as extratropical cyclones with their maximum value of the 12-hr deepening rate ε exceeding 1 hPa/hr (Yoshida and Asuma 2004);

$$\varepsilon = -\frac{p_c(t+6\,\mathrm{hr}) - p_c(t-6\,\mathrm{hr})}{12\,\mathrm{hr}} \frac{\sin 60^\circ}{\sin\phi}, \tag{1}$$

where p_c is the central sea-level pressure of the cyclone, ϕ is the latitude where the central low pressure is located. Kawamura (2011) has analyzed atmospheric reanalysis data, JRA-55 (spacial resolution of $1.25^\circ \times 1.25^\circ$, time interval of 6 hr, data domain), for the past 429 explosive cyclones observed between October 1996 and April 2017 to create a comprehensive database, called Northwest Pacific Megastorm Database (NPMD), of the trajectory, intensity and deepening rate of all cyclones. In this section, meteorological features of the explosive cyclones that passed through the northwestern Pacific Ocean, based on the NPMD, are statistically analyzed in terms of evolution type, as proposed by Yoshida and Asuma (2004).

2.1. *Fundamental features*

Figure 2 shows the distributions of (*a*) the probability of cyclone passage, (*b*) mean speed of cyclones, (*c*) mean central pressure of cyclones p_c, and (*d*) mean deepening rate ε. High passage frequencies of explosive cyclones are recognized along the east coast of Japan over the path of the Kuroshio Current in the Pacific Ocean (see **Figure 2** *a*), indicating that cyclones intensify significantly with upward heat flux from warm seawater in the Kuroshio Current (see also high deepening rates on the current in **Figure 2** *d*). The passage frequencies decrease in land areas due to the lack of heat supply from the ocean, suggesting that heat energy from the ocean enhances explosive cyclogenesis (**Figure 2** *a*). Typical cyclones over both the northwest Pacific Ocean and Sea of Japan travel northeast with a mean speed of 12–13 $\mathrm{m\,s^{-1}}$ (**Figure 2** *b*), which may be comparable to the mean speed of typhoons passing this area (40°N), 11.9 $\mathrm{m\,s^{-1}}$, calculated using Best Track Data provided by Regional Specialized Meteorological Center (Kunitsugu 2012). The travel speed of the cyclones declines significantly over

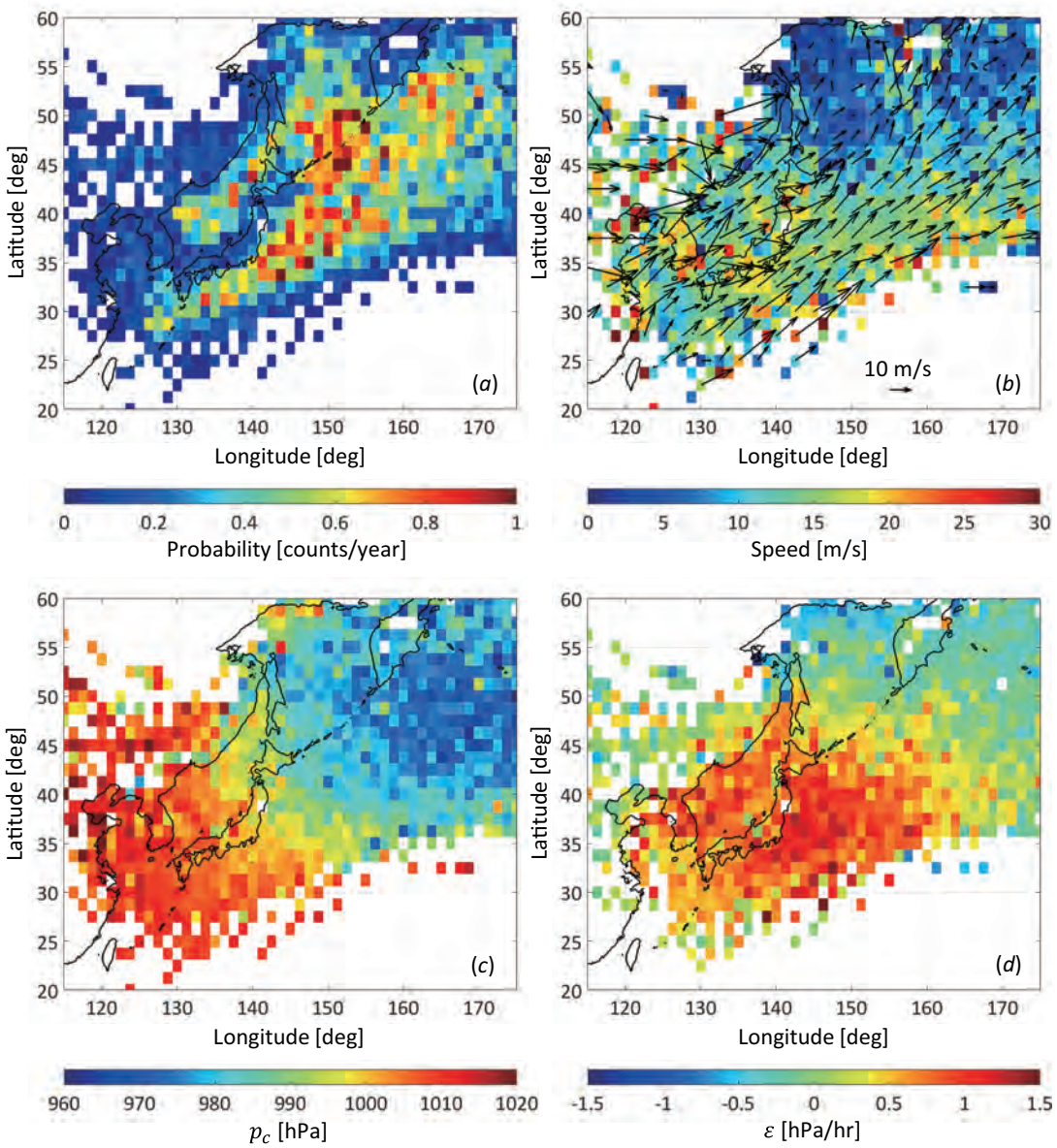

Figure 2. Statistical features of explosive cyclones in the northwest Pacific region. (*a*) probability of cyclone passage, (*b*) mean speed of cyclones in color and velocity in vectors, (*c*) mean central pressure, (*d*) mean deepening rate.

the Sea of Okhotsk, where high passage frequencies are observed (see **Figure 2** *a*), indicating stationary behaviors of the cyclones. This may be caused by an atmospheric blocking effect, which is often observed near northern Okhotsk (Kitano and Yamada 2016).

A high deepening rate, ε, is observed in the Sea of Japan and the west Pacific Ocean (**Figure 2** *d*), and lower ε in the Sea of Okhotsk and the north Pacific Ocean, where fully developed cyclones take the lowest mean central pressure, p_c (**Figure 2** *c*). Accordingly, cyclones formed in the seas adjacent to the Japanese archipelago

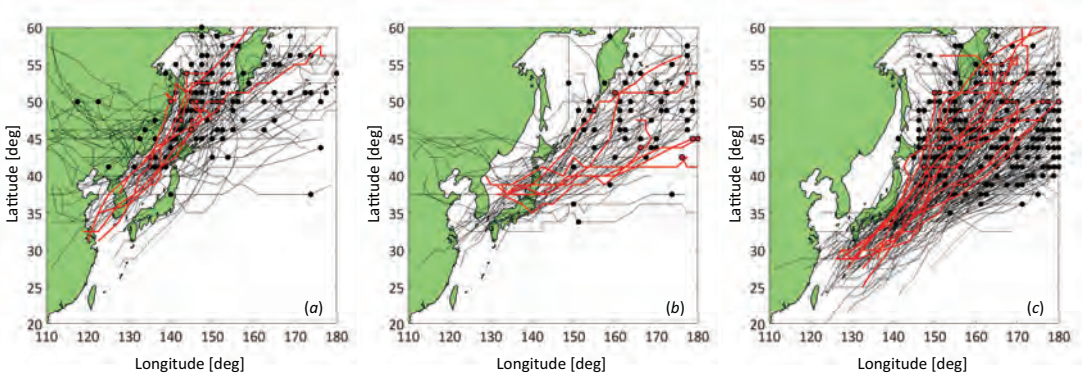

Figure 3. Trajectories of explosive cyclones categorized in (*a*) Type I, (*b*) Type II, and (*c*) Type III. Red lines represent the trajectories used in this study. Circles indicate the locations of the cyclones to achieve the lowest central pressure.

intensify during northeast movement (**Figure 2** *b*) and are fully developed, with maximum strength, when they reach the northern seas of Japan. Because highly intensified cyclones tend to stay in the northern sea (**Figure 2** *b*), violent winter storms may continue for a long time, typically several days, as has been frequently observed along the north coast of Hokkaido (e.g. Kitano and Yamada 2016; Kawano and Kawamura 2018).

2.2. *Types of cyclone evolution*

According to Yoshida and Asuma (2004), the evolution of explosive cyclones in the northwest Pacific area is highly influenced by the activity of the cold Siberian air mass, resulting in seasonal variations in the formation, trajectories and intensification of cyclones, which can be divided into three major types based on their statistical features.

Figure 3 shows all cyclone trajectories of each type from 1996 to 2017, extracted from NPMD (Kawamura 2011), which falls into 126 cyclones of Type I, 64 cyclones of Type II and 255 cyclones of Type III. Explosive cyclones, formed at the end of autumn when the Siberian air mass is weak, developing in the baroclinic zone between the Eurasian continent and Sea of Japan and traveling northeast over the Sea of Japan towards the Sea of Okhotsk, are referred to as Type I in this paper (see **Figure 3** *a*). Type-II cyclones form on the continent, and then move east towards the Pacific Ocean across the Japanese archipelago and turn to the northeast; these are typically observed in the beginning of winter when the continental cold air mass intensifies, affecting the northern portion of Japan (see **Figure 3** *b*). As the Siberian air mass develops fully in midwinter, extending up the east coast of Japan, the formation and movement of cyclones are constrained to an area off the east coast of Japan, referred to as Type III (see **Figure 3** *c*). This type of cyclones, traveling near the Kuroshio Current (see **Figure 1**), may be affected by thermal effects from the current (Yoshida and Asuma

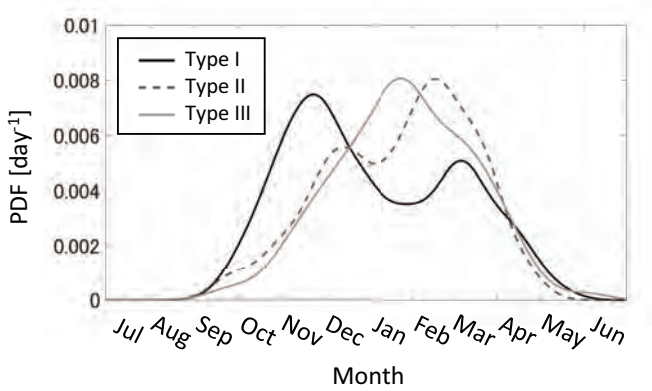

Figure 4. Estimated probability density function of formation frequency of explosive cyclones of each evolution type in 1 year.

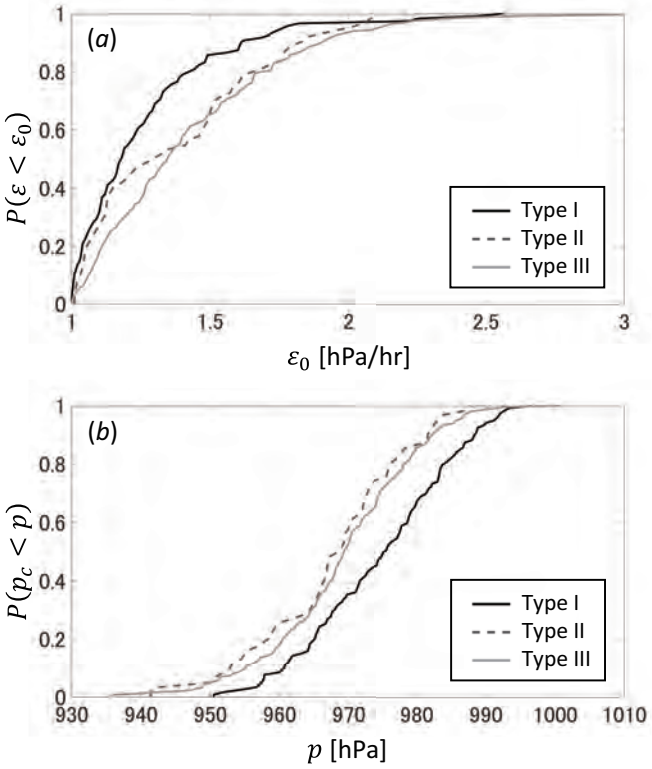

Figure 5. Probabilities of (a) maximum deepening rate ε and (b) minimum central pressure p_c for Type-I, -II and -III explosive cyclones.

2004). Chen et al. (1992) reported that latent heat from the ocean surface contributes greatly to the rapid development of extratropical cyclones in the northwest Pacific, where sea-surface temperature is high due to the Kuroshio warm current. In this case, the major energy source driving intensification of the cyclones may be moisture and latent heat supplied from the warm seawater of the current, rather than baroclinicity. Notably, the storm surges that occurred in Nemuro Bay in 2014 and 2015 (Saruwatari et al. 2015) were caused by Type-III cyclones, as discussed further below.

The probability density functions for formation of explosive cyclones of each type, which was calculated using a normal kernel density estimation (Silverman 1986), are compared in **Figure 4**. The probability density for Type-I cyclones has two local maxima in November and March, when the Siberian air mass is less active. In Type II, two maxima are reached in December and February, when the Siberian High is moderate, while the highest probability of Type-III cyclone formation occurs in January, when the Siberian air mass has its most active period of the year.

Figure 5 shows the probabilities of the maximum deepening rate and minimum central pressure of explosive cyclones. We found that Type-III cyclones traveling on the Pacific Ocean have higher deepening rates than Type-I cyclones passing over the Sea of Japan, because of rapid growth due to latent heat supplied by a warm current in the Pacific Ocean, as discussed above. Type-II cyclones, which pass over the baroclinic zone in the Sea of Japan formed by the moderate extension of the cold air mass and then move over the warm seawater of the Pacific Ocean, exhibit intermediate deepening features (**Figure 5** *a*). The minimum central pressures of Type-III cyclones were 5–10 hPa lower than those of Type-I cyclones with the same probability (**Figure 5** *b*).

The local properties of the storm surges that occur in northeast Asia in winter may depend on these meteorological features of cyclone evolution. We modeled ocean currents under winter cyclones of each major evolution type to identify the statistical features of local sea level responses.

3. Computational Method

In this section, the computational model and conditions used in this study are first explained, and results computed for previous storm surge events are then introduced for validation purposes.

3.1. *Three-dimensional ocean circulation model*

The meso- and regional-scale flows that cause storm surges during explosive cyclones were analyzed using a three-dimensional non-hydrostatic model, the MIT general circulation model (MITgcm, Marshall et al. 1997a,b). This model simultaneously computes the following momentum and continuity equations.

$$\frac{D\boldsymbol{u}_h}{Dt} = -\frac{1}{\rho_c}\boldsymbol{\nabla}_h p + (2\boldsymbol{\Omega}\times\boldsymbol{u})_h + \boldsymbol{F}_{\boldsymbol{u}_h}, \tag{2}$$

$$\frac{Dw}{Dt} = -\frac{1}{\rho_c}\frac{\partial p}{\partial z} + (2\boldsymbol{\Omega}\times\boldsymbol{u})_v + F_w, \tag{3}$$

$$\boldsymbol{\nabla}\cdot\boldsymbol{u} = 0, \tag{4}$$

where $\boldsymbol{u} = (\boldsymbol{u}_h, w)$ are the horizontal and vertical velocities, respectively, p is the pressure, ρ_c is the reference density, $\boldsymbol{\Omega}$ is the Earth's rotation, $\boldsymbol{F}_{\boldsymbol{u}_h}$ and F_w are the

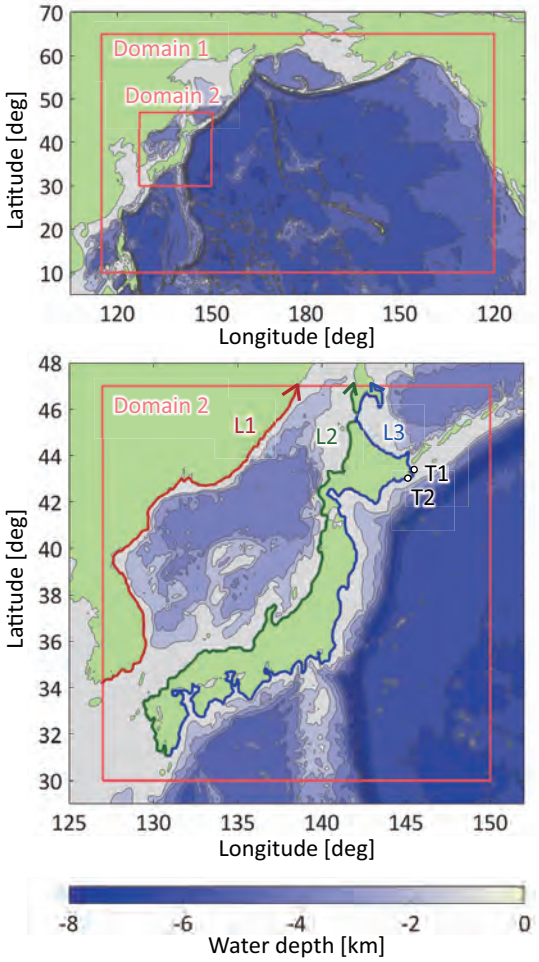

Figure 6. Water depth in the computational domains. $L1$, $L2$ and $L3$ in domain 2 are the axes defined along the east coast of Eurasia, the west coast of Japan and the east coast of Japan, respectively.

horizontal and vertical source terms associated with external forcing and dispersion, and the gradient operator is $\boldsymbol{\nabla} = (\boldsymbol{\nabla}_h, \partial/\partial z)$. Wind stress was given as an external force calculated by a bulk formula of Oey et al. (2006) that was proposed based on the model of Large and Pond (1981) for moderate wind conditions and the data of Powell, Vickery, and Reinhold (2003) for high wind conditions. The surface elevation η was updated by determining mass conservation;

$$\frac{\partial \eta}{\partial t} + \boldsymbol{\nabla}_h \cdot (\eta + H)\, \boldsymbol{u}_h \quad = \quad 0. \tag{5}$$

The details of the computational methods are provided in Marshall et al. (1997a,b).

Two-domain nesting computations were performed from 48 hr prior to the cyclone formation to the end of the storm event in the horizontal domain shown in **Figure 6** and **Table 1**, with the vertical z-coordinate having higher resolution near the ocean surface (minimum grid width of 2.0 m at the surface). The horizontal resolutions were designed to cover large-scale ocean responses to traveling cyclones in domain 1 ($30'$ grid

Table 1. Details of the computational domains.

	Domain 1	Domain 2
Computational domain	10°N–65°N, 115°E–120°W	30°N–47°N, 127°E–150°E
Horizontal resolution	$30' \times 30'$	$10' \times 10'$
Vertical resolution	2.0–698 m	2.0–698 m
Grid number	$251 \times 111 \times 100$	$139 \times 103 \times 100$
Timestep interval	10 sec	10 sec

width) and to resolve local sea level rise in semi-closed coasts enough in domain 2 ($10'$ grid width). Two meteorological datasets were used to estimate the surface boundary conditions of wind stress and sea level pressure; JRA-55 at 1.25° resolution with a 3-hr interval (Kobayashi et al. 2015) for the meso-scale domain 1, and JMA-MSM at 5 km resolution with a 1-hr interval (Saito et al. 2006) for the regional-scale domain 2. We confirmed that the both datasets provides continuous, consistent meteorological data along the domain boundaries. Any effects of astronomical tide and interactions with wind waves were ignored in the computation to focus on a meteorological component of storm surges. The bathymetry was provided by GEBCO_2014 at $30''$ resolution.

3.2. *Validation*

A fully intensified explosive cyclone with minimum central pressure of 946.5 hPa induced the storm surge in Nemuro Bay on December 17, 2014, causing significant flooding in central Nemuro city (see Saruwatari et al. 2015). In this section, the computed sea level is compared with the tide record during the storm event for validation of the current model.

Figure 7 shows the meteorological tide records at Nemuro Port facing Nemuro Bay (T1) and Kiritappu Port facing the Pacific Ocean (T2), compared with the computed sea level at the corresponding locations (see locations in **Figure 1** and **Figure 6**). It should be noted that the astronomical tide has been excluded from the original tide record measured at the ports, to enable fair comparison with the computed results, which have no tide assumption. The sea level began to rise at T1 from 12:00 on December 16 (UTC) and achieved a maximum sea level of 1.6 m at 0:00 on December 17. Because T1 is located in a semi-enclosed basin (Nemuro Bay, see **Figure 1** and **Figure 6**), sea surface rises were the highest with the greatest wind-driven current discharge into the bay and the minimal atmospheric pressure, which was achieved at the cyclone's closest approach to the site (see Saruwatari et al. 2015, for details). According to Saruwatari et al. (2015), which roughly estimated the pressure-induced surge by equivalent water pressure to the local atmospheric pressure and the wind-induced surge by the residual meteorological tide, the pressure-induced component of the maximum sea level rise was about 0.6 m, and the wind-stress-induced component was about 1.0 m in this event. Our model predicts the major features of the observed sea level (**Figure 7** *a*); the identical time when sea level rise began and when the

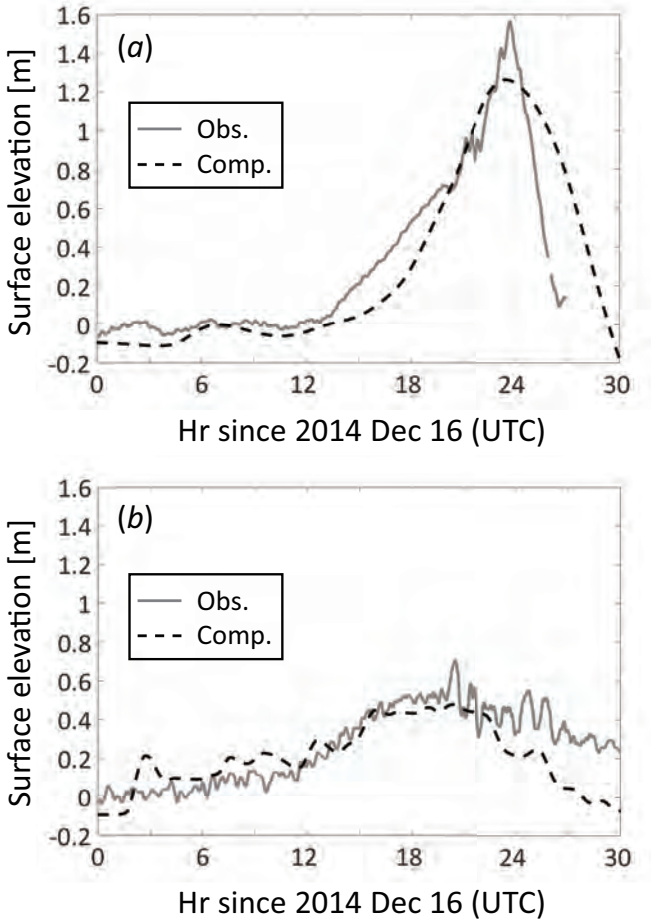

Figure 7. Comparison of the sea levels during the Nemuro storm surge at the observation sites (*a*) T1 and (*b*) T2; observed meteorological tide excluding astronomical tide component in the observed tide record (solid line) and computed sea level (broken line).

maximum sea level was reached, and the maximum sea level, ensuring the validity of the results for both components of sea level rise. At T2, which faces the open ocean (see **Figure 1** and **Figure 6**), only the pressure-induced component might contribute to the increase in sea level rise as the maximum meteorological tide was comparable to the estimated pressure-induced sea level rise. We found that the computed result is consistent with the observed maximum sea level which reinforces the validity of our computational method for predicting pressure-induced sea level rise (**Figure 7** *b*). On the one hand, minor errors after achieving the maximum sea level are observed in the both sites. Kumagai et al. (2017) used a wave-storm-surge coupled model for a hindcasting computation of the same surge event at higher resolution (228 m $\times$ 309 m) than the current one. While overall variations of the computed sea level at T1 was reasonable, the computed maximum sea level was achieved about three hours earlier than the observed one. They mentioned this error might be associated with optional models of sea surface drag force, but substantial causes to induce the error, occurred even in the high resolution computation, have not been identified. One possible fac-

tor causing the errors is an effect of significant inland flooding along the bay coast, which was not assumed in the both current and Kumagai's computations, since the T1 tide observation site in Nemuro port was close to the flooded coast. The explicit effects of flooding to storm surge predictions needs to be identified for improving the computational accuracy in future research.

3.3. *Computational conditions*

In this study, two sets of numerical experiments were performed to see the statistical features of sea level rise due to passages of explosive cyclones observed in the past two decades (**Table 2**), and to evaluate uncertainties of the computed storm surge responding to meteorological ensemble disturbances (**Table 3**).

An extreme cyclone has been often defined to have the intensity higher than the 70th to 90th percentile of total cyclones in a quantile analysis, which well characterizes distinctive developing processes (Elsner, Kossin, and Jagger 2008; Lehmann and Coumou 2015). In this study, an extreme explosive cyclone was defined to have intensity higher than the 80th percentile, in terms of the central pressure and deepening rate. The representative extreme events to be computed were selected from each type of the extreme explosive cyclones derived from NPMD; 6 representative extreme cyclones in Type I (25% of total Type I extreme cyclones), 6 representatives (48%) in Type II and 12 representatives (24%) in Type III, corresponding to 5–7% of the total number of each explosive storm (119 of Type I, 62 of Type II and 248 of Type III) stored in NPMD.

To statistically evaluate the potential dispersion of computed sea levels with respect to meteorological disturbances, additional computations were also performed using meteorological ensembles (JMA-EPS; Ensemble Prediction System) (e.g. Yamaguchi et al. 2009) for two representative extreme events, selected from the extreme cyclones in **Table 3**, which previously caused inland storm disturbances. The cyclone trajectories of all ensemble members used in the computations are shown in **Figure 8**. The uncertainties of the cyclone evolution, depending on the evolution type, may also affect uncertainties of sea level changes during storm surge events, which is discussed in Section 4.

4. Computational Results

In this section, the uncertainty of the storm surge with respect to cyclone trajectories is discussed based on the statistical distributions of sea level rise induced by the ensemble cyclones. Local disaster risks along the coasts of northeast Asia are then discussed in reference to the computed possible sea level rises.

Table 2. Storm events sampled from among all explosive cyclones recorded in the past two decades.

Case	Event period (UTC)	Minimum SLP [hPa]	Maximum deepening rate [hPa/hr]
I-1	48 hr since 20141130 00:00	974.3	1.62
I-2	89 hr since 20171223 00:00	946.7	2.04
I-3	60 ht since 20041126 00:00	950.5	2.56
I-4	70 hr since 20150930 00:00	951.9	2.22
I-5	72 hr since 20120402 00:00	957.8	2.47
I-6	95 hr since 20141030 00:00	957.7	1.35
II-1	60 hr since 20110324 12:00	973.8	1.08
II-2	57 hr since 20101227 12:00	975.6	1.04
II-3	71 hr since 20130319 00:00	950.5	1.76
II-4	38 hr since 20050209 00:00	957.0	2.06
II-5	95 hr since 20150115 00:00	958.9	1.62
II-6	95 hr since 20170204 00:00	959.4	1.51
III-1	47 hr since 20150301 00:00	969.2	1.66
III-2	48 hr since 20150226 00:00	977.9	1.53
III-3	71 hr since 20000319 00:00	951.4	2.63
III-4	71 hr since 20060201 00:00	962.4	2.48
III-5	95 hr since 20130113 00:00	936.1	3.09
III-6	95 hr since 20110313 00:00	941.6	2.08
III-7	95 hr since 20170119 00:00	947.5	1.35
III-8	95 hr since 20100111 00:00	948.9	1.95
III-9	95 hr since 20141228 00:00	949.8	2.13
III-10	95 hr since 20080329 00:00	955.2	2.36
III-11	95 hr since 20070105 00:00	952.9	2.31
III-12	95 hr since 20121229 00:00	960.2	1.73

Table 3. Storm events used for ensemble computations.

Case	Event period (UTC)	Minimum SLP [hPa]	Maximum deepening rate [hPa/hr]	Number of ensemble members
I-1	48 hr since 20141130 00:00	974.3	1.62	26
I-2	89 hr since 20171223 00:00	946.7	2.04	7
II-1	60 hr since 20110324 12:00	973.8	1.08	9
II-2	57 hr since 20101227 12:00	975.6	1.04	8
III-1	47 hr since 20150301 00:00	969.2	1.66	9
III-2	48 hr since 20150226 00:00	977.9	1.53	14

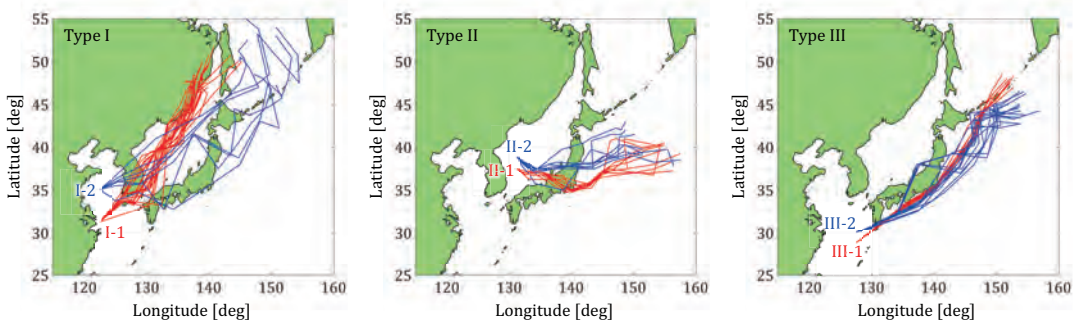

Figure 8. Trajectories of the cyclone ensembles.

4.1. *Statistical analysis of the storm surge ensembles*

If any disturbance is introduced in the original meteorological data, a forecast using the disturbed initial conditions may deviate from the original forecast over the fore-

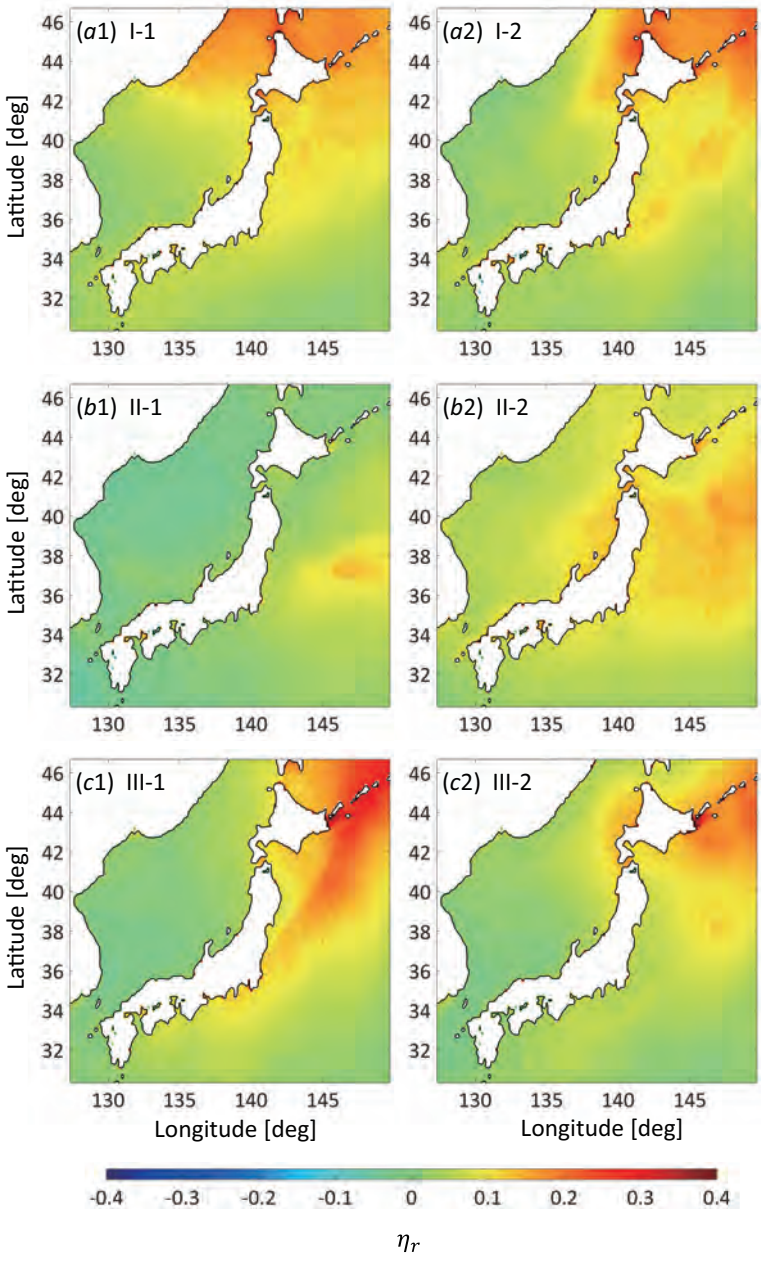

Figure 9. Mean non-dimensional maximum sea level of the storm surge ensembles. (*a*) Type I, (*b*) Type II, and (*c*) Type III.

cast period. Ensemble member cyclones with initial perturbations evolve differently and travel on different trajectories (**Figure 8**), which may result in differing local evolutionary patterns of storm surges. The statistical features of the resulting storm surge ensembles, indicating uncertainty in storm surge prediction as well as possible modification of sea level variation, are discussed for six storm events (cases I-1, I-2, II-1, II-2, III-1, III-2; see **Table 3**) in this section.

The maximum sea level recorded during the 2014 Nemuro storm surge, $\eta_0 = 1.6\,\mathrm{m}$,

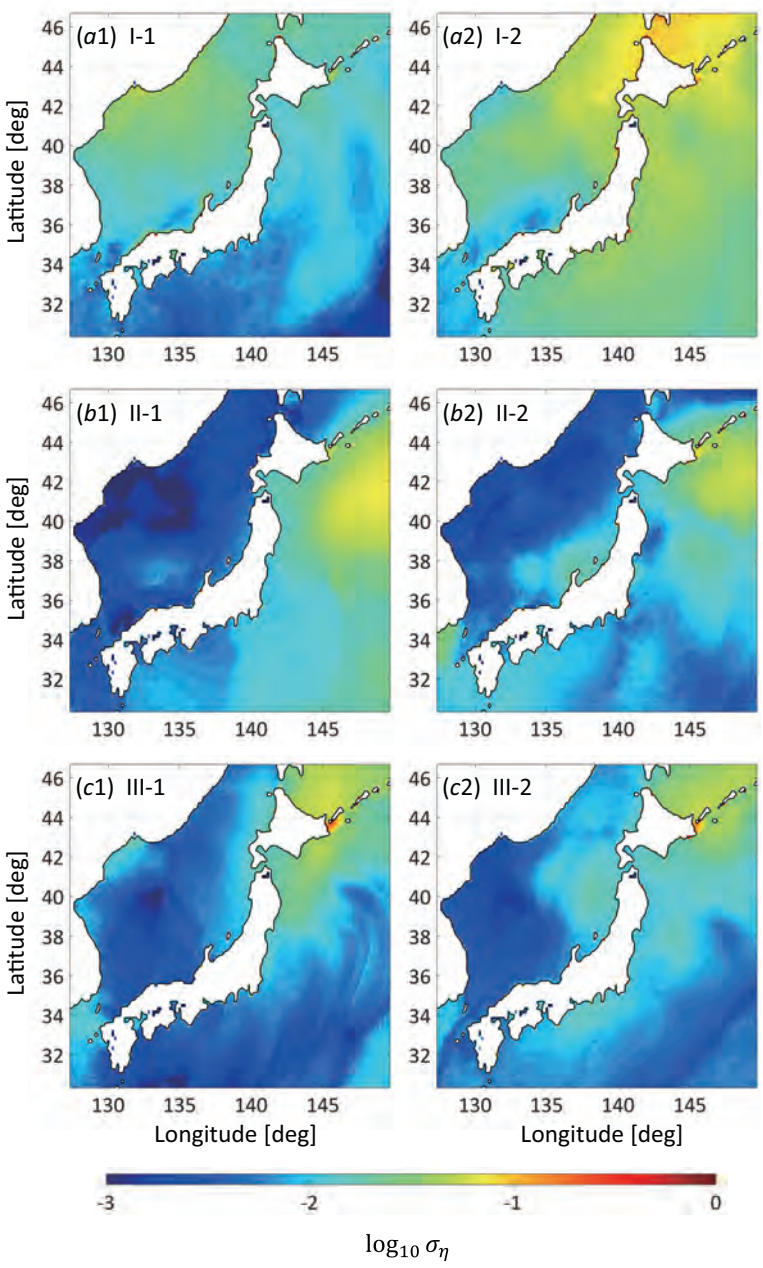

Figure 10. Standard deviation of the non-dimensional maximum sea level for the storm surge ensembles. (a) Type I, (b) Type II, and (c) Type III.

is used as the reference sea level for defining relative mean sea level rise with respect to the highest sea level record due to an explosive cyclone in this area, $\eta_r = \overline{\eta_{\max}}/\eta_0$, where $\overline{\eta_{\max}}$ is the ensemble average of maximum sea level. **Figure 9** shows the relative mean sea level rise, η_r, estimated for each storm event. For Type-I cyclones (see **Figure 9** $a1$ and $a2$), despite the orientation and dispersion of the cyclone trajectories differing significantly between case I-1 and I-2 (see **Figure 8**), the distributions of η_r exhibit analogous in both cases, with higher sea levels extending over an area from the northern

Sea of Japan to the Sea of Okhotsk; the highest local sea levels are achieved in the Soya Strait and Nemuro Bay. The maximum η_r in Type II is lower than the other types (see **Figure 9** $b1$ and $b2$), despite Type-II cyclones being stochastically more energetic than those of Type I (c.f. the lower central pressure and higher deepening rate in **Figure 5**). We found that the highest sea level is localized in Nemuro Bay for both cases III-1 and III-2 (see **Figure 9** $c1$ and $c2$), suggesting a high risk of storm surge disaster along Nemuro Bay, where the first storm surge disaster caused by an explosive cyclone in Japan were recorded. We note that relatively high sea levels are localized in semi-enclosed coastal basins, indicating wind-induced currents entering into a bay from the inlet are trapped on bay-shaped shores to cause amplification of the sea level rise on the shore in addition to the pressure-induced component. The relative locations of the bay inlet and cyclone, that determine the additional sea level rise due to the wind-induced surge, are thus an important factor in predicting potential sea level rise, indicating that local coastal vulnerability should be assessed in terms of characteristic cyclone trajectories, which is the focus of this study.

Figure 10 shows the distributions of the logarithmic standard deviation of the highest relative sea levels, $\sigma_\eta = \sqrt{\overline{(\eta_{max}/\eta_0 - \eta_r)^2}}$, measuring uncertainty of the predicted sea levels due to a possible deviation of a cyclone trajectory. It is noted that higher σ_η values are distributed off the east coast of Hokkaido for Type II, and over the Sea of Okhotsk for Type-III cyclones. In particular, the highest σ_η for Type III is localized in Nemuro Bay, indicating potential amplification of the local sea level.

In summary, ensemble statistics for specific storm events show that the distributions of both η_r and σ_η depend on the evolution type of the explosive cyclone, and that potential vulnerability is anticipated in semi-enclosed basins, especially in Nemuro Bay, where highest η_r and σ_η values are localized.

4.2. *Local vulnerability to storm surges*

In this section, we discuss the local disaster risks of storm surge based on statistical sea level rises during representative events sampled from all storms over the last two decades (see computed cases in **Table 2**). **Figure 11** shows the sample mean ($\eta'_r = \overline{\eta'_{\max}}/\eta_0$) and standard deviation ($\sigma'_\eta = \sqrt{\overline{(\eta_{\max}/\eta_0 - \eta'_r)^2}}$) of the normalized maximum sea level, where $\overline{\eta'_{\max}}$ is the sample average of maximum sea level. The spatial distributions of η'_r exhibit analogous features with the ensemble mean η_r, defined in Section 4.1, depending on the evolution type. In Type-I cyclones, higher η'_r is found in the northern area off Hokkaido, from the north Sea of Japan to the Sea of Okhotsk (see **Figure 11** $a1$), which may be caused by energetic cyclones often remaining in this area, as explained in Section 2.1, where pressure-induced surge may in general be a major cause of sea level rise in the open ocean. During this type of cyclone, sea level rises over 20% of η_0 are expected on Hokkaido coasts facing the Sea of Japan and the Sea of Okhotsk for a single storm event, while potential storm surges are also

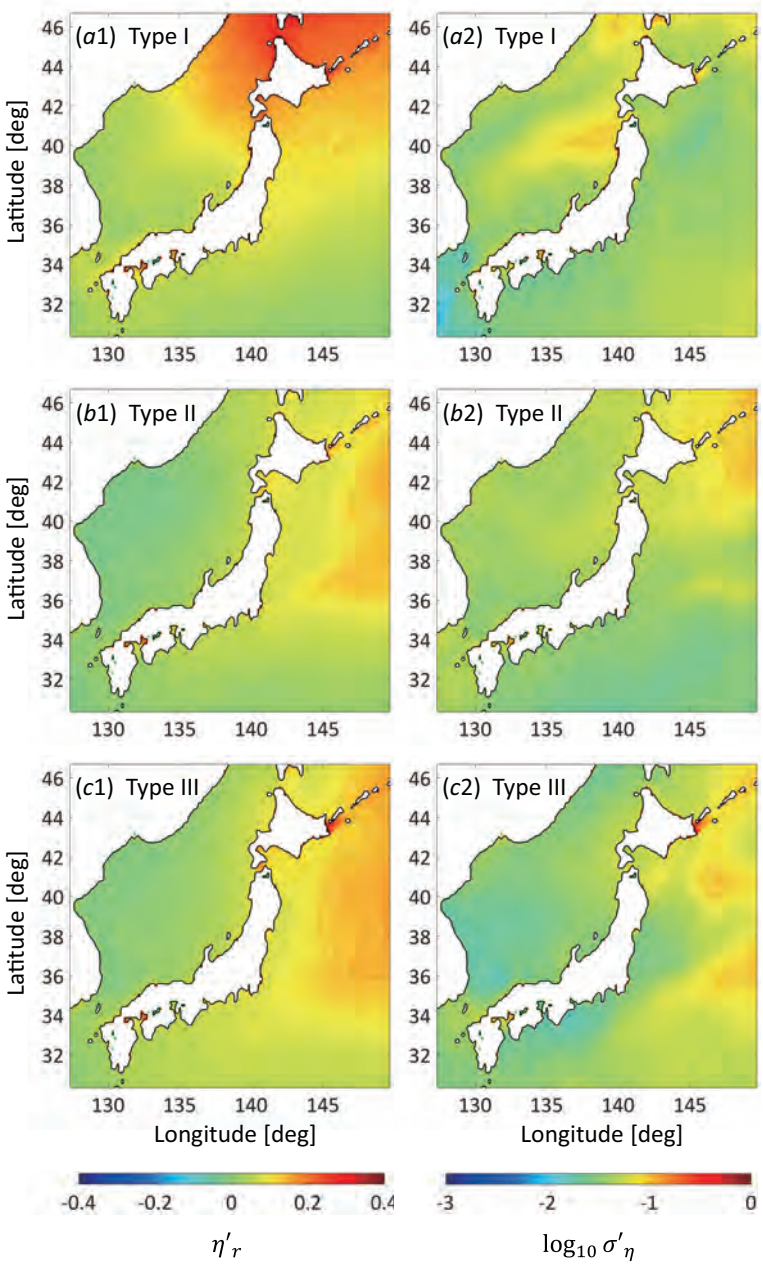

Figure 11. Mean (left) and standard deviation (right) of the non-dimensional maximum sea level during storm events sampled over the last two decades.

expected on coasts facing the Soya Strait, Nemuro Bay and Akita Bay, where attain significantly high standard deviations. Values of η'_r and σ'_η are lower throughout the domain in Type-II cyclones since this type of cyclone tends to achieve the lowest pressure after moving away from the coasts (see **Figure 3**), suggesting a lower storm surge risk than the other types (see **Figure 11** *b*1 and 2). In Type-III storms, η'_r and σ'_η extend off the east coast of Japan along the paths of the cyclones (see **Figure 11** *c*1 and 2). In particular, the highest η'_r and σ'_η values are achieved in Nemuro Bay, where

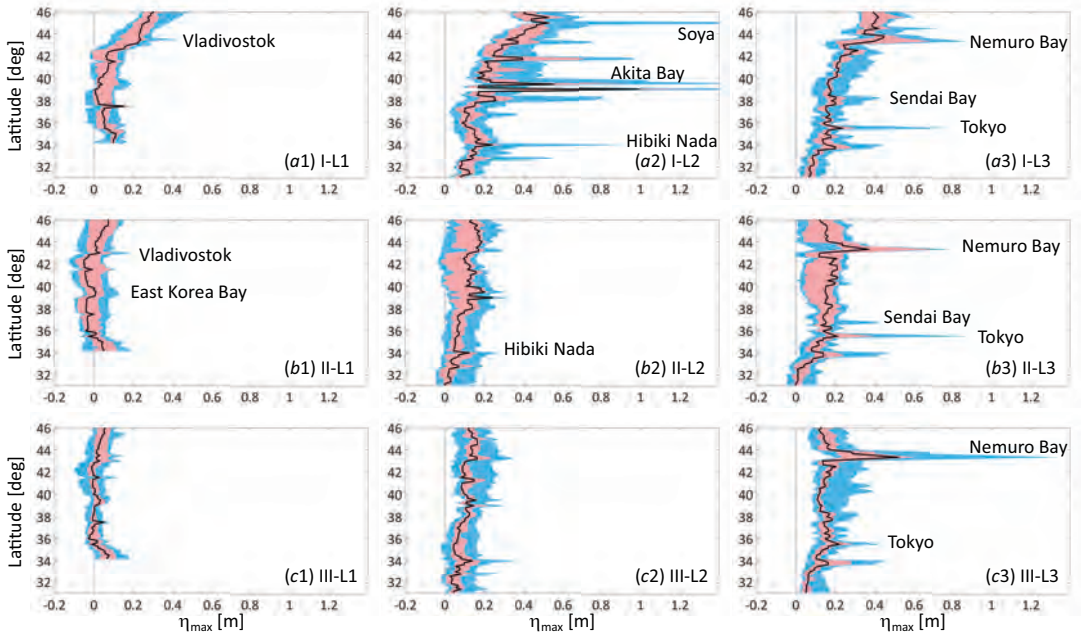

Figure 12. Meridional distribution of the maximum sea level along the axis of L1–L3. (blue) 10th–90th percentile, (pink) 30th–70th percentile and (black) 50th percentile. (*a*) Type I, (*b*) Type II, and (*c*) Type III.

wind-induced surge significantly amplifies sea level rise, indicating that this coast is most vulnerable to the cyclones that form regularly in the northwest Pacific Ocean, and that further extreme storm surges may occur in the bay. It should be noted that the standard deviation in **Figure 11** (*a*2, *b*2 and *c*2) is one-order larger than the one of ensemble experiment in **Figure 10** over the whole domain, indicating the meteorological uncertainty of the surge height is much smaller than the possible height range.

Meridional distributions of the 10th, 30th, 50th, 70th and 90th percentile sea level rise along the east coast of Eurasia, L1, the west coast of Japan, L2, and the east coast of Japan, L3 (see locations of the coasts in **Figure 6**), indicating possible amplification of the sea level rise along the coast, are shown in **Figure 12**. The L1 coast is unaffected by meteorological disturbances of Type II and III cyclones moving away from the coast (see **Figure 3** *b* and *c*), while some Type I cyclones can approach the northern part with higher latitude than 43°N (see **Figure 3** *a*), resulting in a low probability of sea level rise throughout with the highest median sea level less than 0.3 m in the northern coast. The Type I cyclones, traveling through the Sea of Japan, significantly affect the sea levels along the L2 coast (west coast of the Japanese archipelago), as the wind-driven west current may be blocked by the coast to lift the sea surface there, especially in semi-enclosed coasts with inlets facing the direction of the current, such as Akita Bay, where attain probable local maxima of sea levels (**Figure 12** *a*2). In particular, a storm surge comparable to the 2014 Nemuro surge may occur along the coasts of Soya Strait and Akita Bay during this type of storm. On the one hand, we

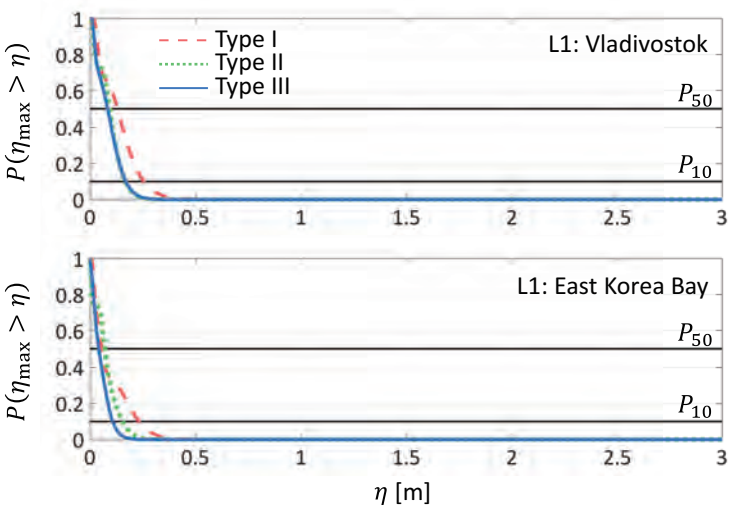

Figure 13. Exceedance probability of the maximum sea level at representative locations along L1 for each type of cyclone passage. 10% and 50% probabilities P_{10} and P_{50} are shown in black lines.

see insignificant sea level rise induced by the other types of cyclones, intensified during the travels in the Pacific Ocean, on the whole L2 coast (**Figure 12** *b*2, *c*2). We also found that among L3 coasts (**Figure 12** *a*3, *b*3, *c*3), Nemuro Bay has a significantly high probability of high sea level rise for any cyclone type, further supporting its high vulnerability regardless of the evolution type. Notably, the 90th percentile sea level rise on semi-enclosed coasts of L2 and L3 are 2–4 times higher than the median value, indicating the possibility to experience extreme storm surges due to the additional wind-driven component, depending on the relative locations of the bay inlet and the cyclone.

An exceedance probability P of the maximum sea level η_{max} on each coast was calculated by a kernel density estimation (Silverman 1986) to the storm-surge samples. **Figure 13** shows the exceedance probability of the sea level rise along the L1 coast. As explained above, the expected sea level rise on this coast is much lower than that along the coasts of Japanese archipelago. The 10% exceedance probabilities for Type I were 0.25 m and 0.23 m in Vladivostok and East Korea Bay, respectively. From **Figure 14**, we see that Soya and Akita Bay have distinctive probability distributions, with long tails for Type-I storms and with elevations of 2.07 m and 1.56 m for the 10% exceedance probability, respectively, which exceed the highest tide recorded during the 2014 Nemuro storm surge. Broad distributions with long tails, with 10% exceedance probabilities of 0.94 m for Type I, 0.91 m for Type II and 1.39 m for Type III, were also found in Nemuro Bay in L3, indicating high likelihood of extreme storm surges (**Figure 15**). Some semi-enclosed coasts, such as Hibiki Nada, Sendai Bay and Tokyo Bay, have local maxima of 10% exceedance probabilities in the range of 0.29 to 0.59 m, suggesting low storm surge risk from any type of explosive cyclone.

We performed a non-parametric Kruskal-Wallis test (Kruskal and Wallis 1952) to obtain stronger evidence of differences in probability distribution for a limited number

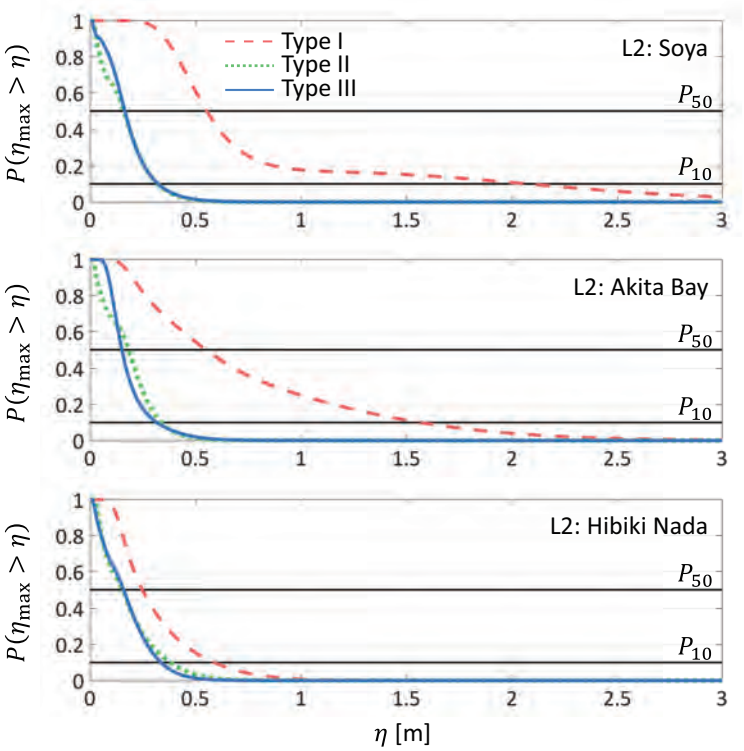

Figure 14. Exceedance probability of the maximum sea level at representative locations along L2 for each type of cyclone passage. 10% and 50% probabilities P_{10} and P_{50} are shown in black lines.

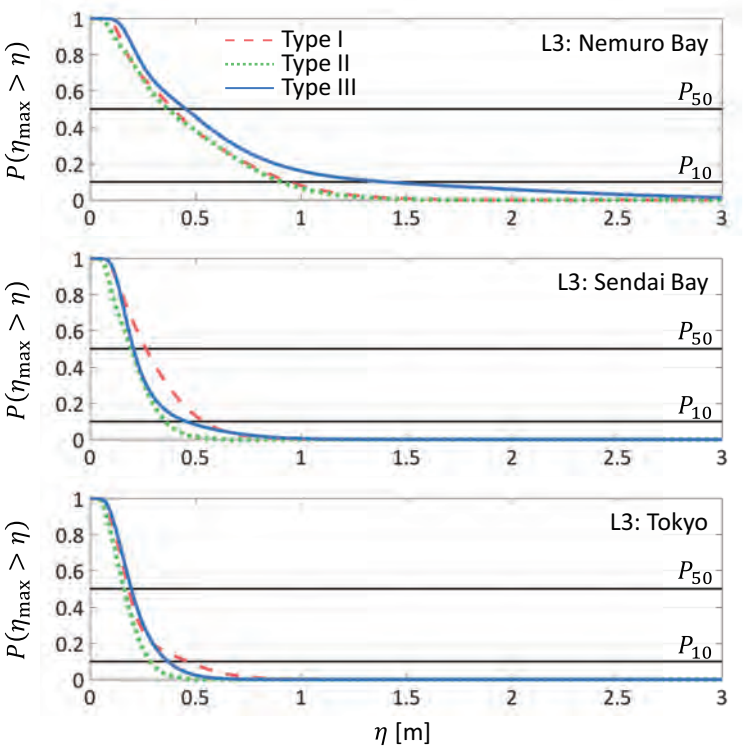

Figure 15. Exceedance probability of the maximum sea level at representative locations along L3 for each type of cyclone passage. 10% and 50% probabilities P_{10} and P_{50} are shown in black lines.

Table 4. Results of the statistical analysis for the maximum sea level due to each type of cyclone.

Location	p-value	Effect size f
Soya	0.17%	0.91
Ishikari Bay	1.96%	0.83
Akita Bay	0.82%	0.95
Nemuro Bay	85.1%	0.23
Vladivostok	36.9%	0.30
Hibiki Nada	30.1%	0.41
Sendai Bay	57.6%	0.25
Tokyo Bay	65.1%	0.22

of the current storm samples for each evolution type. The Kruskal-Wallis test evaluates the null hypothesis that three or more groups of limited sample members have no difference. If the estimated p-value is lower than 5% then there is significant statistical evidence to reject the hypothesis that all three types of groups have no difference; that is, only specific evolution type affects the site. The effect size f measures the difference between average values of the groups; e.g. if $f = 0$ then the average of each groups is identical, and if $f = 1$ then each group average has a difference of the identical value to the standard deviation. The both quantities are summarized in **Table 4**. At Soya, Ishikari Bay and Akita Bay, facing the northeast Sea of Japan, the p-value is less than 5% and the effect size is greater than 0.83, indicating there is sufficient statistical evidence to reject the hypothesis and significant difference in the average; that is, these locations were more vulnerable to the specific, Type-I cyclones than the other types (see also **Figure 14**). The p-values at the other sites are greater than 5%, not rejecting the null hypothesis, indicating possible sea level rise against multiple types of cyclones. In particular, the high p-value in Nemuro Bay (85.1%) and low f there (0.23) indicate that a similar level of storm surge may occur regardless of the evolution type (see also **Figure 15**).

5. Conclusions

In this study, we computationally investigated the statistical features of storm surges induced by explosive cyclones in the northwest Pacific region during winter. Three major evolution types of explosive cyclones, proposed by Yoshida and Asuma (2004), were considered as external forcing factors of a storm surge.

Type-I cyclones formed in early and late winter, traveling northward in the Sea of Japan, leading to significant sea level rise increases over a region of the Sea of Okhotsk and northern Sea of Japan. Type-II cyclones, frequently observed in December and February, travel from the Sea of Japan to the Pacific Ocean across the Japanese archipelago, causing milder sea level changes than seen with other types, as these cyclones move away from the coast before they attain the maximum intensity. Type-

III cyclones often gain latent heat energy from the Kuroshio Current to develop in midwinter, resulting in the highest probability of extreme local amplification of sea level in Nemuro Bay, where previously suffered from the 2014 Nemuro extreme cyclone. Possible local maxima of sea level are found in semi-enclosed coasts with inlets facing the direction of the wind-induced current; that is, the relative locations of the inlets and cyclones, classified by trajectory type, determine the maximum possible sea level and thus the vulnerability of the coast to storm surge. In particular, Nemuro Bay exhibited the highest possible surges for all three evolution types, and is the site most vulnerable to explosive cyclones that develop in the northwest Pacific Ocean. Thus, repeated disasters are anticipated there. We also found that Type-I cyclones may bring a severe storm surge with extreme sea level rise, exceeding that recorded during the 2014 Nemuro storm surge, in semi-enclosed coastal basins along the Sea of Okhotsk and northern Sea of Japan. These findings, describing distinctive statistical responses of storm surges characterized by the three major evolution types of explosive cyclone in the northeast Asia, provide a realistic scenario that is consistent with meteorological characteristics of winter cyclones locally developing there for assessing possible storm surge disasters.

In the northwest Pacific region that was the focus of this study, and where energetic winter cyclones form every year, measures must be introduced to reduce disasters caused by possible storm surges. The probabilistic risk analysis of storm surges due to explosive cyclones, in terms of their typical evolution types as proposed in this study, will be useful for quantifying local vulnerability of any coastal area where analogous explosive cyclones form in addition to the current sites, such as the northwest Atlantic region.

Disclosure Statement

The authors declare no competing interests.

Funding

This research was supported by JSPS Grant-in-Aids for Scientific Research (18H01537, 18H03791).

References

Bricker, Jeremy D., Volker Roeber, Yo Fukutani, and Shuichi Kure. 2015. "Simulation of the December 2014 Nemuro Storm Surge and incident waves." *J. JSCE, Ser. B2 (Coastal Engineering)* 71 (2): 1543–1548.

Catalano, Arielle J., and Anthony J. Broccoli. 2018. "Synoptic Characteristics of Surge-

Producing Extratropical Cyclones along the Northeast Coast of the United States." *Journal of Applied Meteorology and Climatology* 57 (1): 171–184.

Chen, Shou-Jun, Ying-Hwa Kuo, Pai-Zhong Zhang, and Qi-Feng Bai. 1992. "Climatology of Explosive Cyclones off the East Asian Coast." *Monthly Weather Review* 120 (12): 3029–3035.

Elsner, James B., James P. Kossin, and Thomas H. Jagger. 2008. "The increasing intensity of the strongest tropical cyclones." *Nature* 455: 92–95.

Gyakum, John R., and Richard E. Danielson. 2000. "Analysis of Meteorological Precursors to Ordinary and Explosive Cyclogenesis in the Western North Pacific." *Monthly Weather Review* 128 (3): 851–863.

Iwao, Koki, Masaru Inatsu, and Masahide Kimoto. 2012. "Recent changes in explosively developing extratropical cyclones over the winter Northwestern Pacific." *J. Climate* 25: 7282–7296.

Kawamura, Ryuichi. 2011. "Northwestern Pacific Megastorm Database." Accessed 2018-05-01. `http://fujin.geo.kyushu-u.ac.jp/`.

Kawano, Tetsuya, and Ryuichi Kawamura. 2018. "Influence of Okhotsk Sea Ice Distribution on a Snowstorm Associated with an Explosive Cyclone in Hokkaido, Japan." *SOLA* 14: 1–5.

Kitano, Yoshikazu, and Tomohito J. Yamada. 2016. "The Comparison between Explosive Cyclone and Typhoon over Northern Japan in the Current and Future Climate." *Procedia Engineering* 154: 726–732.

Kobayashi, S., Y. Ota, Y. Harada, A. Ebita, M. Moriya, H. Onoda, K. Onogi, et al. 2015. "The JRA-55 reanalysis: General specifications and basic characteristics." *J. Meteor. Soc. Japan* 93: 5–48.

Kocin, Paul J., Philip N. Schumacher, Ronald F. Morales, and Louis W. Uccellini. 1995. "Overview of the 12–14 March 1993 Superstorm." *Bulletin of the American Meteorological Society* 76 (2): 165–182.

Kruskal, William H., and W. Allen Wallis. 1952. "Use of Ranks in One-Criterion Variance Analysis." *Journal of the American Statistical Association* 47 (260): 583–621.

Kumagai, Kenzo, Sooyoul Kim, Daiki Tsujio, Hajime Mase, and Takahito Tsuji. 2017. "Coupled modeling of wave and storm surge for explosive cyclone 2014 in the east coast of Hokkaido (in Japanese)." *J. JSCE, Ser. B2 (Coastal Engineering)* 73 (2): 193–198.

Kunitsugu, Masashi. 2012. "Tropical Cyclone Information Provided by the Rsmc Tokyo - Typhoon Center." *Tropical Cyclone Research and Review* 1 (1): 51–59.

Kuwano-Yoshida, Akira, and Yoshio Asuma. 2008. "Numerical Study of Explosively Developing Extratropical Cyclones in the Northwestern Pacific Region." *Monthly Weather Review* 136 (2): 712–740.

Large, W. G., and S. Pond. 1981. "Open Ocean Momentum Flux Measurements in Moderate to Strong Winds." *J. Phys. Oceanogr.* 11 (3): 324–336.

Lehmann, J., and D. Coumou. 2015. "The influence of mid-latitude storm tracks on hot, cold, dry and wet extremes." *Sci. Rep.* 5: 17491.

Marshall, J., A. Adcroft, C. Hill, L. Perelman, and C. Heisey. 1997a. "A finite-volume, incompressible Navier Stokes model for studies of the ocean on parallel computers." *J. Geophys. Res. Oceans* 102, C3: 5753–5766.

Marshall, J., C. Hill, L. Perelman, and A. Adcroft. 1997b. "Hydrostatic, quasi-hydrostatic, and nonhydrostatic ocean modeling." *J. Geophys. Res. Oceans* 102, C3: 5733–5752.

Oey, L.-Y., T. Ezer, D.-P. Wang, S.-J. Fan, and X.-Q. Yin. 2006. "Loop Current warming by Hurricane Wilma." *Geophys. Res. Lett.* 33 (8): L08613.

Parise, Cláudia Klose, Lauro Júlinelio Calliari, and Nisia Krusche. 2009. "Extreme storm surges in the south of Brazil: atmospheric conditions and shore erosion." *Brazilian Journal of Oceanography* 57: 175–188. `http://www.scielo.br/scielo.php?script=sci_arttext&pid=S1679-87592009000300002&nrm=iso`.

Powell, Mark D., Peter J. Vickery, and Timothy A. Reinhold. 2003. "Reduced drag coefficient for high wind speeds in tropical cyclones." *Nature* 422: 279–283.

Saito, Kazuo, Tsukasa Fujita, Yoshinori Yamada, Jun-ichi Ishida, Yukihiro Kumagai, Kohei Aranami, Shiro Ohmori, et al. 2006. "The Operational JMA Nonhydrostatic Mesoscale Model." *Monthly Weather Review* 134 (4): 1266–1298.

Sanders, Frederick. 1986. "Explosive Cyclogenesis in the West-Central North Atlantic Ocean, 1981–84. Part I: Composite Structure and Mean Behavior." *Monthly Weather Review* 114 (10): 1781–1794.

Sanders, Frederick, and John R. Gyakum. 1980. "Synoptic-Dynamic Climatology of the "Bomb"." *Monthly Weather Review* 108 (10): 1589–1606.

Saruwatari, Ayumi, Adriano Coutinho de Lima, Masaya Kato, Osamu Nikawa, and Yasunori Watanabe. 2015. "Report on the 2014 Winter Cyclone Storm Surge in Nemuro, Japan." *Coastal Engineering Journal* 57 (3): 1550014–1–1550014–14.

Silverman, Bernard. W. 1986. *Density Estimation for Statistics and Data Analysis*. Chapman & Hall.

Yamaguchi, Munehiko, Ryota Sakai, Masayuki Kyoda, Takuya Komori, and Takashi Kadowaki. 2009. "Typhoon Ensemble Prediction System Developed at the Japan Meteorological Agency." *Monthly Weather Review* 137 (8): 2592–2604.

Yoshida, Akira, and Yoshio Asuma. 2004. "Structures and Environment of Explosively Developing Extratropical Cyclones in the Northwestern Pacific Region." *Monthly Weather Review* 132 (5): 1121–1142.